Available online at www.sciencedirect.com
SCIENCE DIRECT
Journal of Catalysis 238 (2006) 277–285
JOURNAL OF CATALYSIS
www.elsevier.com/locate/jcat

Thermolytic molecular precursor route to site-isolated vanadia–silica materials and their catalytic performance in methane selective oxidation

Daniel A. Ruddy [a,b], Nicholas L. Ohler [b,c], Alexis T. Bell [b,c], T. Don Tilley [a,b,*]

[a] *Department of Chemistry, University of California, Berkeley, CA 94720–1461, USA*
[b] *Chemical Sciences Division, Lawrence Berkeley National Laboratory, 1 Cyclotron Road, Berkeley, CA 94720, USA*
[c] *Department of Chemical Engineering, University of California, Berkeley, CA 94720–1462, USA*

Received 9 July 2005; revised 22 November 2005; accepted 23 November 2005

Available online 18 January 2006

Abstract

The thermolytic molecular precursor (TMP) method was used to prepare site-isolated, high-surface area vanadia–silica (V/SBA15) materials of various V loadings via the grafting of two precursors, $OV[OSi(O^tBu)_3]_3$ (**1**) and $OV(O^tBu)_3$ (**2**). Spectroscopic analysis indicates that excellent synthetic control was established for the exclusive formation of a pseudotetrahedral monovanadate (VO_4) structure on all catalyst surfaces. Another V/SBA15 catalyst was prepared via conventional incipient wetness impregnation (WI) with aqueous NH_4VO_3. A spectroscopic investigation of this catalyst revealed the presence of monovanadate and polyvanadate species along with small domains of V_2O_5. The TMP materials behave as single-site catalysts in the selective oxidation of methane to formaldehyde up to a V coverage of 0.47 $V\,nm^{-2}$ and demonstrate superior activity compared with the WI catalyst. A space–time yield of 5.84 $kg_{CH_2O}\,kg_{cat}^{-1}\,h^{-1}$ was observed, more than twice the highest value previously reported.

Keywords: Vanadia–silica; Monovanadate; Thermolytic molecular precursor method; Single-site catalyst; Methane selective oxidation

1. Introduction

Advances in heterogeneous catalysis continue to play an important role in the world economy. The structure of the active sites on these catalysts are often not well-defined, presenting a formidable synthetic task for chemists and materials scientists in designing new, high-performance catalysts. It has been demonstrated that good activity and selectivity often stem from active sites consisting of one or only a few isolated metal centers [1–4]. Maintaining synthetic control over the catalyst nanostructure and characterizing the active sites are therefore essential to the establishment of structure–activity relationships for catalyst development [5].

The direct conversion of methane to more valuable commodity chemicals, such as methanol and formaldehyde, is one of the most challenging issues in catalysis research [6]. The significance of developing an efficient catalyst for this methane selective oxidation reaction has escalated in recent years due to the increasing concern over fossil fuel consumption. Although various catalysts have been used in the oxidation of light alkanes to oxygenates, supported vanadia catalysts have exhibited particularly promising results for numerous hydrocarbon substrates (e.g., cyclohexane, cyclohexene, toluene, methanol). Spectroscopic studies suggest that isolated pseudotetrahedral monovanadate (VO_4) species often lead to better catalytic performance [7–10]. The preparation of vanadia–silica catalysts using conventional wetness impregnation (WI) methods with aqueous $NaVO_3$ or NH_4VO_3 on silica (surface area 300–500 $m^2\,g^{-1}$) can, however, result in the formation of numerous surface species, including isolated VO_4, polymeric V_xO_y, and bulk V_2O_5 even at relatively low V loadings [11–13]. To eliminate the formation of V_2O_5 without reducing the loading of V to levels that are difficult to control, several investigators have turned to the use of high-surface area (700–1000 $m^2\,g^{-1}$) ordered mesoporous silicas such as MCM41 and SBA15 [14–16]. Although impregnation of these

* Corresponding author.
E-mail address: tdtilley@berkeley.edu (T.D. Tilley).

0021-9517/$ – see front matter
doi:10.1016/j.jcat.2005.11.032

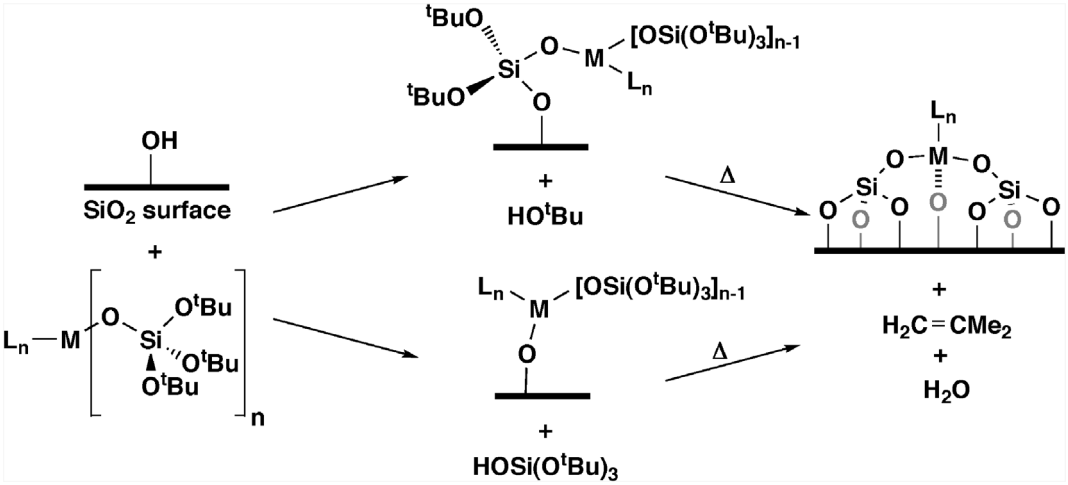

Scheme 1. Thermolytic molecular precursor approach to surface-supported, isolated active sites.

supports with vanadate salts has lead to a greater abundance of monovanadate and polyvanadate species relative to bulk vanadia, precise control of V speciation has not been achievable.

A recently developed technique for the preparation of well-defined isolated metal centers is based on the *thermolytic molecular precursor* (TMP) method. In this approach, oxygen-rich metal siloxide complexes are grafted onto a metal oxide support via a protonolysis reaction, followed by low-temperature (<473 K) calcination to remove the remaining hydrocarbons (Scheme 1) [17]. This route has been successfully applied for the preparation of site-isolated Ti(IV), Fe(III), and Ta(V) species that display remarkable catalytic activity and/or selectivity in hydrocarbon oxidation [18–20]. Molecular precursors are also useful as model compounds of supported active sites, allowing for detailed structural and spectroscopic analyses.

The molecular precursor $OV[OSi(O^tBu)_3]_3$ (**1**) was previously synthesized and characterized as an excellent spectroscopic model compound for isolated pseudotetrahedral VO_4 sites on silica [21]. Here we report the nonaqueous grafting of **1** onto the surface of SBA15 to yield vanadia–silica materials. The grafting of a less sterically hindered molecular precursor, $OV(O^tBu)_3$ (**2**), is also reported. For direct spectroscopic and catalytic comparison, a vanadia–silica material was prepared via incipient WI with NH_4VO_3. The nature of the supported vanadia species was determined by various techniques, and the catalytic performance of these materials in the selective oxidation of methane to formaldehyde was evaluated.

2. Experimental

2.1. General

All manipulations were conducted under a nitrogen atmosphere using standard Schlenk techniques or in a Vacuum Atmospheres drybox, unless otherwise noted. Dry, oxygen-free solvents were used throughout. Benzene-d_6 was purified and dried by vacuum distillation from sodium/potassium alloy. Solution ^{1}H nuclear magnetic resonance (NMR) spectra were recorded at 400 MHz using a Bruker AVQ-400 spectrometer. Chemical shifts for ^{1}H NMR spectra were referenced internally to the residual solvent proton signal relative to tetramethylsilane. Trichlorovanadium(V) oxide was purchased from Strem Chemicals and distilled before use. The following were prepared according to literature procedures: SBA15 [22], $(^tBuO)_3SiOH$ [23], $OV[OSi(O^tBu)_3]_3$ [21], and $OV(O^tBu)_3$ [24]. The mesoporous support, SBA15, was characterized by powder X-ray diffraction (XRD) and N_2 porosimetry before catalyst preparation (surface area, 630–790 $m^2\,g^{-1}$; pore volume, 0.65–1.14 $cm^3\,g^{-1}$; average pore diameter, 7.6–9.4 nm). The hydroxyl group concentration of the SBA15 was determined to be 2.0(1) OH nm^{-2} via reaction of SBA15 with $Mg(CH_2C_6H_5)_2 \cdot 2THF$ and quantification of the toluene evolved by ^{1}H NMR spectroscopy [25].

2.2. Catalyst preparation

The molecular precursors **1** and **2** were prepared as described previously, and their purity was verified via NMR spectroscopy and elemental analysis [21,24]. Solution ^{1}H NMR spectroscopy was used to monitor the grafting reaction of **1** and **2** onto the SBA15 surface. The reaction of a solution of **1** with SBA15 at room temperature for 24 h resulted in the elimination of only trace amounts of $HOSi(O^tBu)_3$; thus little grafting occurred. On heating the reaction of **1** with SBA15 at 343 K for 24 h, $HOSi(O^tBu)_3$ (1.0 eq. based on disappearance of **1** from solution) and HO^tBu (0.1 eq.) were observed. These elimination products suggest the grafting reaction given in Eq. (1), with ca. 90% of the surface-bound species retaining two siloxide ligands and a small amount binding to the surface through one of the siloxide ligands after elimination of HO^tBu. The maximum V loading attainable using precursor **1** corresponded to ca. 0.28 V nm^{-2} (1.4 wt%; based on the disappearance of **1** from

the solution):

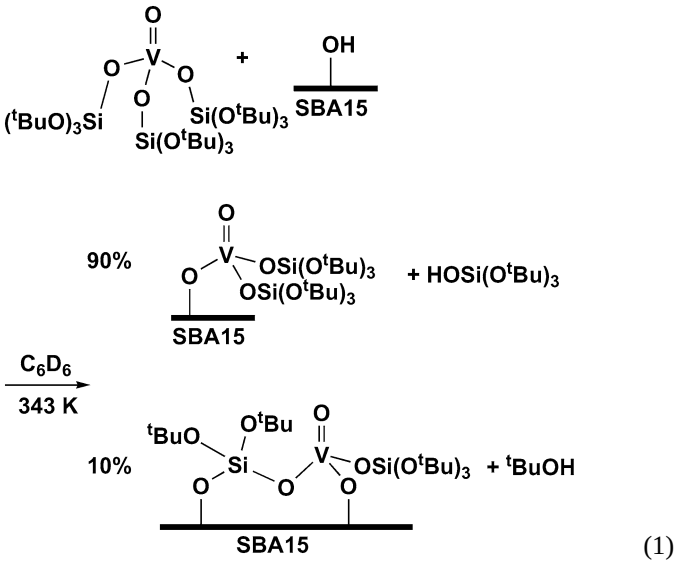

(1)

The reaction of a solution of **2** with SBA15 at room temperature for 24 h produced HO^{t}Bu (1.0 eq.) as the sole elimination product. This implies that the surface-supported species retained two *tert*-butoxy ligands, as given in Eq. (2). The maximum V loading attainable using precursor **2** was ca. 1.0 V nm^{-2} (7.0 wt%, based on the disappearance of **2** from the solution). These NMR-scale experiments suggest that the grafting of small amounts of **1** or **2** results in site-isolated VO_4 centers [18–20]:

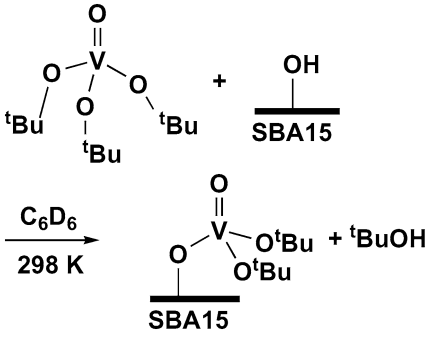

(2)

For catalyst preparation, the molecular precursors were grafted onto the silica support by adding a hexane solution of **1** or **2** to a stirred hexane suspension of SBA15 and heating at reflux (342 K). The V wt% loading was controlled by the concentration of precursor added to the reaction. After 20 h, the solid was isolated by filtration and dried in vacuo for 1 h at room temperature. The grafted materials were calcined at 873 K (10 K min^{-1}, 4 h of soaking) under flowing air. On exposure to ambient conditions for a few minutes, the catalysts changed from colorless to yellow, a color change previously attributed to water adsorption [26]. For this reason, the materials were dried in vacuo at 393 K for 12 h and handled under a nitrogen atmosphere. The weight loss observed by thermogravimetric analysis (TGA) and combustion analysis (EA) before calcination was comparable to the calculated values based on the grafting chemistry observed by ^{1}H NMR spectroscopy. Carbon was undetectable by EA (<0.4%) after calcination.

For direct comparison, a catalyst was prepared via conventional incipient WI of SBA15 with a solution of NH_4VO_3 at a pH of ca. 2, and the solvent was evaporated for 16 h at 318 K. The sample was oven-dried at 383 K for 24 h and calcined at 873 K (10 K min^{-1} heating rate, 4 h of soaking) under flowing air. The series of catalysts are referred to as V_RSBA15(x), where R denotes the precursor used (R = Si denotes precursor **1**, R = C denotes precursor **2**, and R = W denotes WI with NH_4VO_3) and x is the wt% of V as determined from inductively coupled plasma (ICP) metal analysis.

2.3. Catalyst characterization

Nitrogen adsorption isotherms were obtained using a Quantachrome Autosorb 1, and samples were outgassed at 393 K for at least 15 h before measurement. The Brunauer–Emmet–Teller (BET) method [27] was used to determine surface areas, and the Barrett–Joyner–Halenda (BJH) method [28] was used to obtain pore size distributions. Thermal analyses were performed on a TA Instruments SDT 2960 Integrated TGA/DSC analyzer with a heating rate of 10 K min^{-1} under an oxygen flow. Carbon and hydrogen elemental analyses were performed at the microanalytical laboratory of the College of Chemistry, University of California Berkeley. Vanadium elemental analyses were performed at Galbraith Laboratories (Knoxville, TN) using ICP methods.

Powder XRD experiments were performed on a Siemens D5000 X-ray diffractometer using Cu-K_α radiation. Transmission electron microscopy (TEM) was carried out on a Philips Tecnai 12 transmission electron microscope operating at 100 kV. Samples for TEM studies were prepared by depositing a hexanes suspension of the catalyst onto carbon-coated copper sample holders obtained from Ted Pella, Inc.

Raman spectra were recorded using a HoloLab series 5000 Raman spectrometer from Kaiser Optical equipped with a Nd:YAG laser that is frequency-doubled to 532 nm and operated at a power of 30 mW measured at the sample with an Edmund Scientific power meter. The resolution of the spectrometer is 1 cm^{-1}. Samples were pressed into 9-mm-diameter wafers at 35 MPa and placed onto a rotating sample holder located within a quartz cell. To reduce laser heating, the samples were rotated at 100 rpm. All samples were pretreated for 2 h at 673 K in moisture-free air flowing at 50 cm^3 min^{-1} through the Raman cell.

Diffuse reflectance UV–vis spectra were recorded using a Varian-Cary 4 spectrophotometer equipped with a Harrick diffuse-reflectance attachment. Samples analyzed before catalytic testing were dehydrated in situ for 2 h at 673 K under a flow of dried air and allowed to cool to room temperature before measurement. Samples analyzed after catalytic testing were dehydrated in situ for 45 min at 423 K under a flow of dried He and allowed to cool to room temperature before measurement. MgO was used as the reference background material.

Table 1
Nitrogen physisorption data and V coverage for the SBA15 support and V_RSBA15 materials

	S_{BET} (m^2 g^{-1})	r_p (nm)	V_p ($cc\,g^{-1}$)	V (nm^{-2})
SBA15	630–790	3.8–4.7	0.65–1.14	0
V_{Si}SBA15(0.40)	480	3.3	0.57	0.10
V_{Si}SBA15(0.68)	470	3.3	0.55	0.17
V_{Si}SBA15(0.98)	430	3.3	0.52	0.27
V_CSBA15(0.42)	640	3.9	0.94	0.08
V_CSBA15(0.79)	630	3.9	0.93	0.15
V_CSBA15(2.4)	590	3.9	0.87	0.47
V_CSBA15(3.5)	480	3.9	0.75	0.85
V_WSBA15(1.7)	470	3.4	0.73	0.43

2.4. Catalytic activity

The flow reaction system used in this study has been described previously [29]. In an inert atmosphere glovebox, 50 mg of catalyst was supported on a plug of quartz wool (ca. 50 mg) in a quartz microreactor. The reactor was designed to minimize the heated volume downstream of the catalyst bed, thereby minimizing the homogeneous oxidation of formaldehyde. The reactor has an i.d. of 4 mm throughout the bed and an i.d. of 2 mm below the bed. After the reactor was connected to the flow manifold, the catalyst was dehydrated under 20% O_2 in He at 873 K for 2 h before the reactants were introduced. The reactant flow composition was 20/10/70 or 90/10/0 CH_4/O_2/He, and the reaction temperature was 873 or 898 K. Pressure was not controlled and was slightly greater than atmospheric. Pressure was accounted for in the calculation of contact time, which was calculated as described previously [29]. The contact time was varied from ca. 0.2 to 0.5 s. The background catalytic activity of unmodified SBA15 was negligible in terms of both methane conversion (<1.0%) and formaldehyde yield (<0.1%) over the range of contact times used to test the catalysts.

3. Results and discussion

3.1. Catalyst characterization

The pore size distribution and surface area of all catalysts were investigated by nitrogen porosimetry. The wt% V loadings, BET surface areas, pore radii, and pore volumes of the SBA15 supports and V_RSBA15 catalysts are given in Table 1. The isotherms of all samples exhibited a type IV hysteresis similar to that of unmodified SBA15, indicating that the mesoporous structure of the material was retained after grafting and calcination. The narrow distribution of pore radii was also preserved. The BET surface areas and average pore radii of the materials decreased on grafting of the precursors and calcination, as observed with previous postsynthetic surface chemistry [18,20,30]. The surface areas of the catalysts prepared using **1** (430–480 m^2 g^{-1}) were smaller than those of the catalysts prepared using **2** (480–640 m^2 g^{-1}), because the SBA15 used with **1** had a lower initial surface area.

Low-angle powder XRD experiments were used to further probe the catalyst pore structure. Diffraction patterns for all catalysts exhibited an intense peak near 2θ values of ca. 0.95°. Peaks in this area were assigned to the (100) reflection due to the long-range ordering of the SBA15 hexagonal pore structure [22]. The presence of this peak provides additional confirmation that the ordered, hexagonal pore structure was retained throughout the grafting/impregnation process and calcination at 873 K.

Wide-angle powder XRD measurements were performed to investigate the presence of any crystalline species in the materials. The diffraction patterns for all catalysts were characteristic of unmodified SBA15; they exhibited no diffraction peaks in the range of 2θ values of 5–70°. No bulk V_2O_5 crystallites larger than ca. 5 nm formed during grafting or calcination. On calcination to 1273 K under air, no crystalline V_2O_5 was detected for the TMP catalysts. TEM also did not reveal any nanometer-scale particles (Fig. 1). The TEM micrographs of the TMP materials confirm that the hexagonal pore structure of the SBA15 remained intact after the grafting and calcination procedure, with no crystallites observed in or around these pores. TEM micrographs of the WI catalyst reveal a stark difference with the TMP materials. Although support particles resembling unmodified SBA15 and the TMP catalysts were present, a number of support particles exhibited an altered morphology indicative of collapse of the mesoporous structure of SBA15, as seen in Fig. 1b. The ratio of particle morphologies could not be determined reliably from these images; however, the nitrogen porosimetry and low-angle powder XRD data suggest that the fraction of collapsed particles is minor.

Although Raman spectroscopy may not be a reliable method for differentiating between monomeric and polymeric surface vanadia species on silica [31], it can be used to reliably iden-

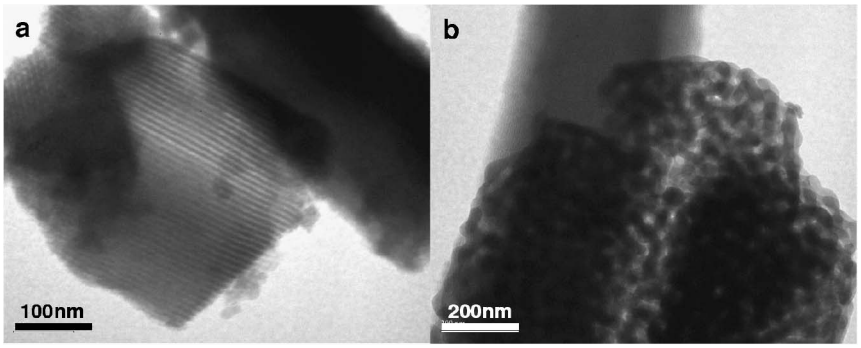

Fig. 1. (a) A typical TEM micrograph of the TMP catalysts and (b) collapsed silica particle observed in the V_WSBA15(1.7) sample.

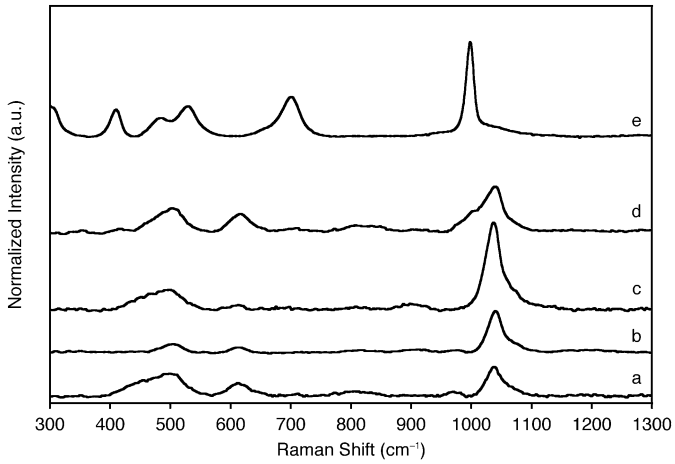

Fig. 2. Raman spectra of (a) V_{Si}SBA15(0.98), (b) V_CSBA15(2.4), (c) V_CSBA15(3.5), (d) V_WSBA15(1.7), and (e) V_2O_5.

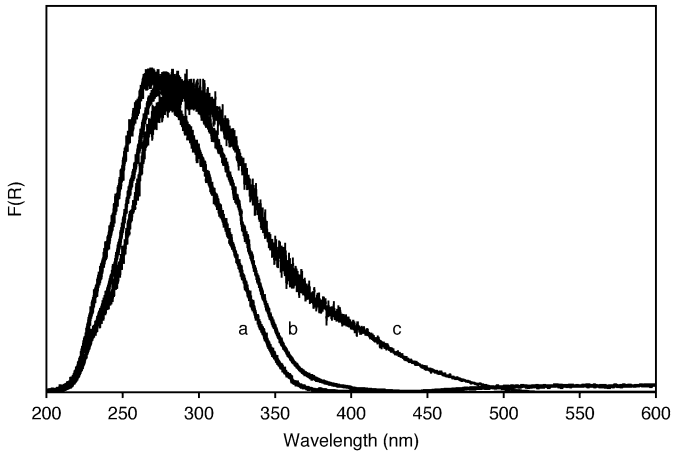

Fig. 3. DRUV–vis spectra of (a) V_{Si}SBA15(0.98), (b) V_CSBA15(2.4), and (c) V_WSBA15(1.7).

tify crystalline V_2O_5, because the scattering cross-section for V_2O_5 (998 cm^{-1}) is estimated to be tenfold that of noncrystalline vanadia (1038 cm^{-1}) [32]. UV–vis spectroscopy can be used to characterize the connectivity of VO_x deposited on oxide supports, because the $O^{2-} \rightarrow V^{5+}$ charge transfer band (LMCT) energy decreases with increasing V–O coordination [26,33–36].

Because of the low V loadings of three of the V_RSBA15 catalysts, Raman scattering spectra with acceptable signals were obtained only for materials of 0.79 wt% V and higher. Fig. 2 presents these spectra along with a V_2O_5 reference spectrum. Adsorbed water is known to alter the Raman spectrum of supported vanadia species [32], so the sample was pressed into a pellet and dehydrated at 673 K for 2 h before the measurement. The spectra contain characteristic peaks of the silica support at 500, 610, and 975 cm^{-1} [33,37]. The most intense peak, centered at 1038 cm^{-1}, is assigned to the $O_3V{=}O$ stretching vibration of noncrystalline vanadia on silica as reported in numerous studies [31,38–41]. As observed in the reference spectrum, crystalline V_2O_5 exhibits characteristic Raman peaks that are easily resolved from noncrystalline vibrations and are observed at 998, 700, and 525 cm^{-1}. Because the Raman scattering cross-section is much greater for V_2O_5 than for monovanadate and polyvanadate, the absence of V_2O_5 peaks in the spectra for the TMP materials is strong evidence that no bulk V_2O_5 is present. It is expected that lower vanadium loadings will lead to better-dispersed vanadia, so formation of V_2O_5 would be less likely in these catalysts because more extensive diffusion must occur before nucleation and grain growth of a crystalline phase [42–44]. Thus V_{Si}SBA15(0.40), V_{Si}SBA15(0.68), and V_CSBA15(0.42) are thought to have similar surface structures, as suggested by the Raman spectra in Fig. 2.

The Raman spectrum of the WI catalyst, V_WSBA15(1.7), is also given in Fig. 2. The peak at 1038 cm^{-1} is still the most dominant feature; however, a shoulder to this peak is also observed, possibly due to the presence of a small amount of crystalline V_2O_5. The lower-frequency peaks of V_2O_5 appear to be broad, suggesting that only a small amount of this species exists, and, considering the powder XRD and TEM data, the crystallites must be small (<5 nm).

DRUV–vis spectroscopy is a more useful technique for differentiating between the three surface species of dehydrated vanadia–silica materials. The energy of the LMCT band shifts to lower energy with increasing vanadium coordination number [38,39,41,45]. The solution UV–vis spectrum of the tetrahedral four-coordinate model compound **1** exhibits an absorbance maximum centered at 250 nm [21]. The UV–vis spectra of vanadate salts have also been investigated to correlate the observed LMCT bands with their known vanadium coordination environment. Tetrahedrally coordinated vanadium ions in Na_3VO_4 exhibit LMCT bands centered at 253 and 294 nm, and the same ion in $Mg_3V_2O_8$ exhibits LMCT maxima at the similar values of 260 and 303 nm [46–49]. Polymeric VO_4 units, as in NH_4VO_3 and $NaVO_3$, exhibit red-shifted LMCT bands at 288/363 and 281/353 nm, respectively [50,51]. Bulk vanadium oxide, which contains vanadium in a distorted octahedron environment, exhibits a broad LMCT band centered at 480 nm [52].

Previous investigations of vanadia supported on mesoporous silica such as MCM41 and SBA15 have used deconvolution of the DRUV–vis spectra as a way to distinguish between different V environments [15,16,33,45]. The experimentally observed spectra were fit with a number of Gaussian curves centered near 240 and 315 nm to represent isolated VO_4 units and curves centered at 320 or 360 nm corresponding to polymeric V_xO_y. The spectra presented in those reports consisted of broad LMCT bands extending past 400 nm. From these data, the band maximum observed at 270–280 nm was attributed to isolated VO_4 units, and a band maximum near 300 nm was assigned to a combination of monovanadates with some polyvanadates and/or V_2O_5. The LMCT absorbance maxima for the TMP materials were observed at 260–285 nm, consistent with the assignment of this band to isolated pseudotetrahedral VO_4 surface species. These materials exhibited narrow LMCT bands with little to no absorbance for wavelengths >400 nm (Fig. 3). This is in contrast to the WI material, which exhibited a broader LMCT band with considerable absorbance up to 500 nm. This LMCT band broadening is attributed to a considerable amount of polymeric

Table 2
Absorption edge energy reference values and experimental values for all V_RSBA15 catalysts

	V nm^{-2}	E_{edge} (eV)
1	–	4.2[a]
Monovanadate	–	3.51
Polyvanadate	–	3.22
V_2O_5	–	2.36
V_{Si}SBA15(0.40)	0.10	3.61
V_{Si}SBA15(0.68)	0.17	3.65
V_{Si}SBA15(0.98)	0.27	3.69
V_CSBA15(0.42)	0.08	3.64
V_CSBA15(0.79)	0.15	3.60
V_CSBA15(2.4)	0.47	3.62
V_CSBA15(3.5)	0.85	3.60
V_WSBA15(1.7)	0.43	3.44

[a] Hexanes solution [21].

V_xO_y and the presence of small domains of V_2O_5, consistent with the Raman scattering spectra.

A more quantitative analysis of the DRUV–vis spectra can be made by comparing absorption edge energies, E_{edge}. This method was discussed by Gao and Wachs [53] and used by Amano et al. for V/SiO_2 catalysts [54]. It has been demonstrated that the edge energy is directly related to the number of covalent V–O–V bonds in the structure. The local coordination of the surface species can be estimated in comparison with reference values determined from ionic vanadate complexes. Table 2 gives the edge energy values of the V_RSBA15 materials as determined through extrapolation of a linear fit to the low-energy edge of a curve of $(F(R)_\infty h\nu)^2$ versus $h\nu$. This table also gives the accepted values associated with each type of vanadium coordination and the experimental value of the model compound **1** [21,53]. The TMP materials exhibited E_{edge} values ranging from 3.61 to 3.69 eV, greater than the value associated with isolated VO_4 units in ionic complexes but consistent with previous observations assigned to monovanadates on silica [53,54]. The edge energy of the WI catalyst was considerably lower, at 3.44 eV, consistent with the presence of polyvanadates and/or V_2O_5 along with monovanadates.

Considering semiquantitative treatments of the DRUV–vis spectra and the Raman scattering, powder XRD, and TEM data, it appears that the nonaqueous grafting of molecular precursors **1** and **2** resulted in excellent synthetic control of the final surface vanadium structure, with monovanadates as the predominant surface species. Conventional WI offered less synthetic control and led to the formation of polyvanadates and crystalline V_2O_5 at relatively low V loadings, as well as to some collapse of the SBA15 pore structure.

3.2. Catalyst performance in methane selective oxidation

The reaction pathways available during methane selective oxidation are given in Scheme 2. Methane is oxidized to formaldehyde or directly to CO_x with rate constants k_1 or k_2, respectively, and formaldehyde is decomposed or oxidized to yield CO_x with rate constant k_3 [55]. The relative importance of the primary and secondary processes for CO_x formation given

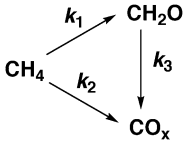

Scheme 2. Oxidation pathways for methane over V/SiO_2 catalysts.

in Scheme 2 were investigated by varying the total flow rate at 873 K with a feed composed of 20% CH_4/10% O_2/70% He. The flow rate was increased to approach zero methane conversion, to estimate the initial selectivity $(k_1/(k_1+k_2))$. Fig. 4a shows how product selectivity changed with methane conversion. Extrapolation to zero methane conversion yielded an initial formaldehyde selectivity of 91%. Thus, most of the CO_x observed at finite methane conversion resulted from secondary processes, such as formaldehyde decomposition and oxidation. The results in Fig. 4a are consistent with those reported previously [8,56].

The effects of V loading and precursor composition on catalytic performance are presented in Fig. 4b. For V loadings of 0.08–0.47 V nm^{-2}, V surface concentration had no effect on TMP catalysts. But increasing the surface concentration to 0.85 V nm^{-2} led to a loss in formaldehyde selectivity at a

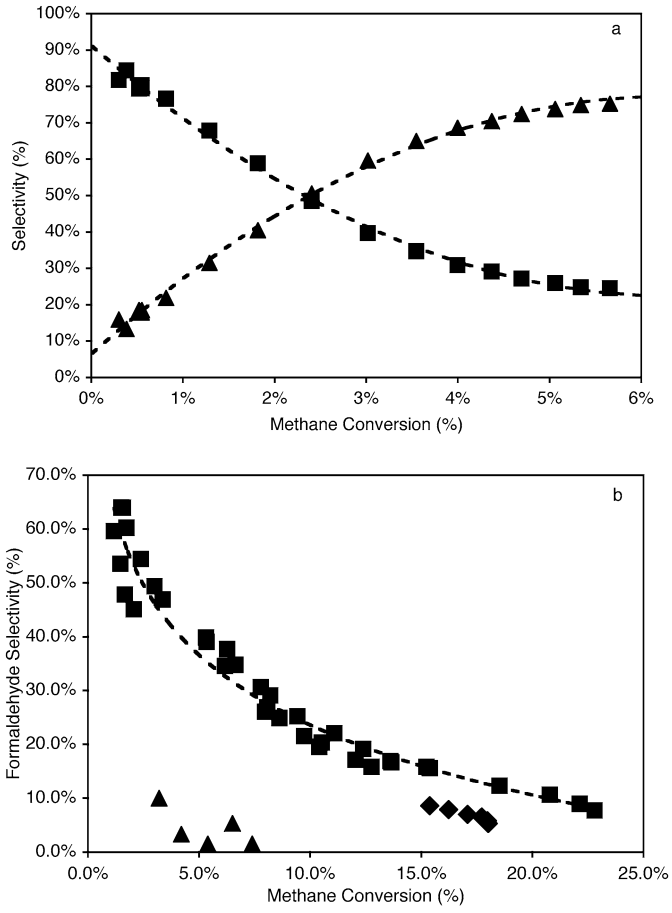

Fig. 4. (a) Formaldehyde (■) and CO_x (▲) selectivity versus methane conversion for V_{Si}SBA15(0.98) at 873 K with feed composed of 20% CH_4/10% O/70% He. (b) Formaldehyde selectivity versus methane conversion for TMP catalysts with 0.08–0.47 V nm^{-2} (■), 0.85 V nm^{-2} (◆), and WI catalyst with 0.43 V nm^{-2} (▲) at 873 K with feed composed of 20% CH_4/10% O_2/70% He.

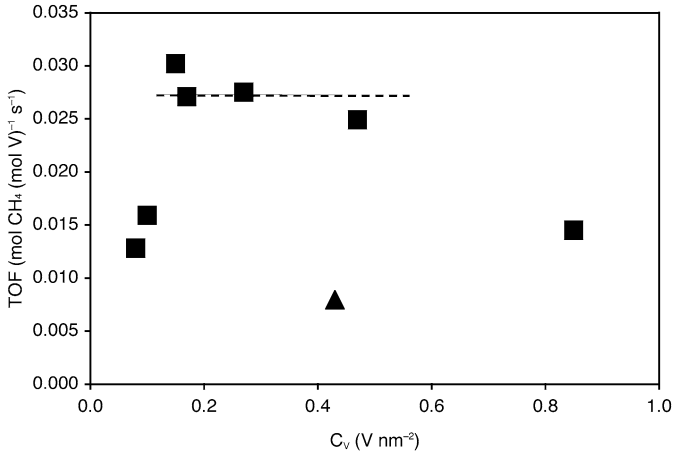

Fig. 5. Methane turnover frequency versus V coverage for TMP (■) and WI (▲) catalysts at 873 K with feed composed of 20% CH_4/10% O_2/70% He.

fixed methane conversion. This effect is significantly more pronounced for the WI catalyst with a surface concentration of 0.43 V nm^{-2}. These results, taken together with those from catalyst characterization, indicate that maintaining high formaldehyde selectivity requires that the dispersed vanadia be present as isolated VO_4 species. Although characterization suggested that the vanadia existed exclusively as monovanadates for all TMP catalysts, the loss of formaldehyde selectivity exhibited by the V_CSBA15(3.5) catalyst is presumed to occur due to the formation of polyvanadates under reaction conditions. This is consistent with results of Bañares et al. [57] at high V coverage (0.8 V nm^{-2}) under reducing conditions, such as those resulting from methane-rich atmospheres. DRUV–vis analysis of the material after a catalytic run resulted in an E_{edge} value of 3.49 eV (vs. 3.60 eV for the fresh catalyst). TMP materials of lower V loading exhibited identical E_{edge} values after catalytic testing. This 0.11 eV drop in edge energy supports the assignment of some V agglomeration on the V_CSBA15(3.5) material during catalysis, leading to lower formaldehyde selectivity.

Fig. 5 plots the activity of the TMP and WI catalysts at 873 K with a feed composed of 20% CH_4/10% O_2/70% He as the methane turnover frequency (TOF) versus vanadium surface concentration (C_V). The methane TOF of the TMP catalysts was approximately constant at a value of 0.027 s^{-1} with respect to vanadium concentrations ranging between 0.15 and 0.47 V nm^{-2}. This demonstrates that as the V loading was varied over this range with the TMP synthetic method, the resulting V sites were uniform. This finding is consistent with the exclusive observation of monovanadate for loadings as high as 0.47 V nm^{-2}. The methane TOF was less for V_CSBA15(3.5) and V_WSBA15(1.7), consistent with V agglomeration on these catalysts in agreement with selectivity-conversion data. The methane TOF was also less for TMP catalysts at low V loadings ($\leqslant$0.10 V nm^{-2}). The reason for this is uncertain, but a similar deviation has been previously reported for V/SiO_2 catalysts, where it was speculated that this deviation indicates cooperation between nearby V sites in the mechanism of methane selective oxidation [58]. The TMP method resulted in a methane TOF of 0.025 s^{-1} for the V_CSBA15(2.4) catalyst, about three times greater than the methane TOF of 0.0080 s^{-1} for the V_WSBA15(1.7) catalyst of similar V coverage prepared by the conventional WI method.

The TMP catalysts of 0.98 and 2.4 wt% V exhibited a formaldehyde single-pass yield of ca. 2.4% at methane conversions in the range of 8–15%. The yield was lower over the V_CSBA15(3.5) catalyst, again indicating the presence of polyvanadates on this catalyst. Table 3 lists the methane conversion (X_{CH_4}), formaldehyde single-pass yield (Y_{CH_2O}), space–time yield (STY), and gas hourly space velocity (GHSV) of the best TMP catalyst V_CSBA15(2.4), the WI catalyst, and previously reported vanadia–mesoporous silica catalysts. For unknown reasons, our WI catalyst did not perform as well as has been reported previously, so the V/SBA15 catalyst reported previously [16] serves as a good basis for comparison to the best TMP catalyst because it has similar V weight loading and was evaluated at similar reaction conditions. The TMP catalyst consisted of isolated monovanadates (vide supra), but the previously reported V/SBA15 catalyst also contained polyvanadates on its surface [16]. As expected from the surface structure, the TMP catalyst produced a greater formaldehyde yield and STY.

Previous researchers studying V/SiO_2 catalysts obtained high STYs of formaldehyde by operating at high GHSV [14–16,59]. To compare catalytic activity with these reports, data were gathered at similarly high GHSV. The resulting STY values from the TMP catalysts were markedly higher. Fig. 6 displays the STY values exhibited by the V_CSBA15(2.4) catalyst over a range of GHSV values under conditions similar to those reported by Berndt et al. [15] and under more methane-rich conditions similar to those reported by Fornes et al. [16]. In both experiments, the TMP catalyst exhibited a greater STY than the previously reported catalysts, while maintaining a formaldehyde yield >1% (Table 4). Under methane-rich conditions, a maximum STY of 5.84 kg_{CH_2O} kg_{cat}^{-1} h^{-1} was obtained. This

Table 3
Performance of V_RSBA15 catalysts and comparable V/SiO_2 catalysts

	V (wt%)	CH_4:O_2	T (K)	X_{CH_4} (%)	S_{CH_2O} (%)	Y_{CH_2O} (%)	STY (g kg_{cat}^{-1} h^{-1})	GHSV (L kg_{cat}^{-1} h^{-1})	References
V/SBA15	1.7	1.0	898	4.6	80.4	3.70	600.0	144,000	[14]
V/MCM41	2.8	5.7	899	5.4	22.0	1.19	1383	180,000	[15]
V/SBA15	2.7	2.0	873	11.2	11.9	1.33	160.2	46,800	[16]
V_CSBA15(2.4)	2.4	2.0	873	15.2	15.8	2.41	224.3	35,300	This work
V_CSBA15(2.4)	2.4	9.0	873	7.1	20.0	1.41	560.5	35,500	This work
V_WSBA15(1.7)	1.7	2.0	873	3.1	14.0	0.44	45.83	35,800	This work
V_WSBA15(1.7)	1.7	9.0	873	2.5	21.4	0.54	245.2	34,700	This work

Table 4
Performance of V_RSBA15 catalysts at high GHSV compared to previously reported V/SiO_2 catalysts

	V (wt%)	T (K)	CH_4:O_2	X_{CH_4} (%)	S_{CH_2O} (%)	Y_{CH_2O} (%)	STY ($g\,kg_{cat}^{-1}\,h^{-1}$)	GHSV ($L\,kg_{cat}^{-1}\,h^{-1}$)	TOF ($mol_{CH_4}\,mol_V^{-1}$) s^{-1}	References
V/MCM41	2.8	899	5.7	4.7	26.1	1.23	1700	225,000	0.145	[15]
V_CSBA15(2.4)	2.4	898	5.7	4.7	32.6	1.53	2282	221,300	0.416	This work
V/SBA15	3.9	891	8.0	1.5	40.0	0.60	2383	417,000	0.0799	[16]
V_CSBA15(2.4)	2.4	898	9.0	5.1	24.3	1.25	5837	403,000	0.480	This work

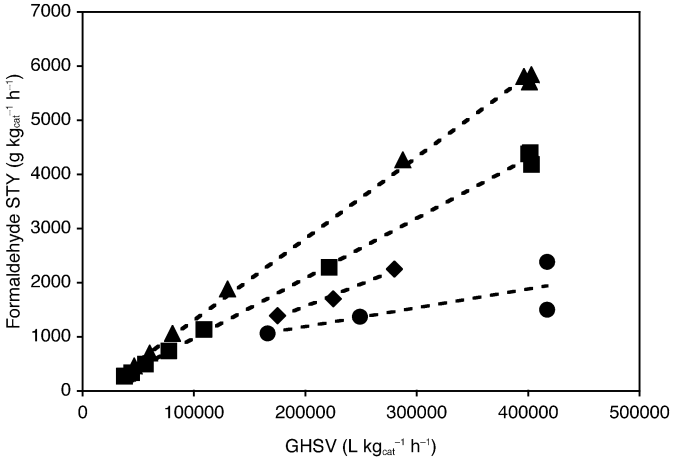

Fig. 6. Space–time yield versus gas hourly space velocity for V_CSBA15(2.4) catalyst at 898 K with feed composed of 57% CH_4/10% O_2 (■) and 90% CH_4/10% O_2 (▲) compared to those of V/SBA15 (◆) and V/MCM41 (■) catalysts under similar operating conditions reported previously by Berndt et al. [15] and Fornes et al. [16], respectively. Data of Berndt et al. collected at 899 K; data of Fornes et al collected at 891 K.

value is more than twice the previously reported highest value and is attributed in part to the excellent synthetic control of the surface V environment through the TMP method. The STY was also enhanced as a result of the increased pressure that built up to drive the fast flows. Although the absolute pressure in the reactor was <1.7 atm under the typical flow conditions used to gather data in this study, the absolute pressure approached 2.3 atm under the high flow rate conditions necessary to achieve high GHSV. This increases the gas–solid contact time and the partial pressures of reactants, both of which are expected to result in greater STY. Similar reactor designs were used by Berndt et al. [15] and Fornes et al. [16], and although the total pressures reported were atmospheric, the pressure increase is needed to drive the fast flows used in those studies as well. Because total pressure was not controlled in any of these studies, comparison of the STY values obtained in different studies is inexact. Nonetheless, Fig. 6 clearly shows that the TMP catalysts outperforms the previously reported catalysts at lower GHSV under conditions at which the pressure drop across the catalyst is negligible.

4. Conclusion

Grafting of the molecular precursors $OV[OSi(O^tBu)_3]_3$ and $OV(O^tBu)_3$ into the pores of SBA15 by the TMP method selectively yielded uniform, site-isolated, tetrahedral VO_4 units for V loadings as high as 0.47 V nm^{-2}. Significant evidence for the presence of isolated, stabilized catalytic centers was obtained by DRUV–vis experiments. These isolated monovanadates are highly active for oxidation of methane to formaldehyde by molecular O_2 and are more active and selective than the polyvanadates resulting from the conventional WI technique. Catalysts prepared by the TMP method displayed superior activity compared with conventionally prepared catalysts of similar V coverage. A space–time yield of 5.84 $kg_{CH_2O}\,kg_{cat}^{-1}\,h^{-1}$ was obtained, more than twice the highest previously reported value.

Acknowledgments

This work was supported by the Director, Office of Energy Research, Office of Basic Energy Sciences, Chemical Sciences Division, of the US Department of Energy under Contract DE-AC03-76F00098 and the Methane Conversion Cooperative sponsored by BP. The authors also thank the A.M. Stacy and E. Iglesia research groups at the University of California Berkeley for allowing the use of their instrumentation (PXRD, DRUV–vis).

References

[1] P. Marturano, L. Drozdova, A. Kogelbauer, R. Prins, J. Catal. 192 (2000) 236.
[2] L.J. Lobree, I.C. Hwang, J.A. Reimer, A.T. Bell, Catal. Lett. 63 (1999) 233.
[3] R. Joyner, M. Stockenhuber, J. Phys. Chem. B 103 (1999) 5963.
[4] M.G. Clerici, P. Ingallina, J. Catal. 140 (1993) 71.
[5] T.D. Tilley, J. Mol. Catal. A 182 (2002) 17.
[6] T. Shimamura, K. Okumura, K. Nakagawa, T. Ando, N.O. Ikenga, T. Suzuki, J. Mol. Catal. A 211 (2004) 97.
[7] M.M. Koranne, J.G. Goodwin, G. Marcelin, J. Catal. 148 (1994) 388.
[8] K. Tabata, Y. Teng, T. Takemoto, E. Suzuki, M.A. Bañares, M.A. Peña, J.L.G. Fierro, Catal. Rev.-Sci. Eng. 44 (2002) 1.
[9] F. Arena, A. Parmaliana, Acc. Chem. Res. 36 (2003) 867.
[10] J.M. Thomas, R. Raja, D.W. Lewis, Angew. Chem. Int. Ed. 44 (2005) 6456.
[11] M.M. Koranne, J.G. Goodwin, G. Marcelin, J. Catal. 148 (1994) 369.
[12] M.A. Bañares, L.J. Alemany, M.L. Granados, M. Faraldos, J.L.G. Fierro, Catal. Today 33 (1997) 73.
[13] C.B. Wang, R.G. Herman, C.L. Shi, Q. Sun, J.E. Roberts, Appl. Catal. A 247 (2003) 321.
[14] B.M. Lin, X.X. Wang, Q. Guo, W. Yang, Q.H. Zhang, Y. Wang, Chem. Lett. 32 (2003) 860.
[15] H. Berndt, A. Martin, A. Bruckner, E. Schreier, D. Muller, H. Kosslick, G.U. Wolf, B. Lucke, J. Catal. 191 (2000) 384.
[16] V. Fornes, C. Lopez, H.H. Lopez, A. Martinez, Appl. Catal. A 249 (2003) 345.
[17] K.L. Fujdala, T.D. Tilley, J. Catal. 216 (2003) 265.
[18] J. Jarupatrakorn, J.D. Tilley, J. Am. Chem. Soc. 124 (2002) 8380.
[19] C. Nozaki, C.G. Lugmair, A.T. Bell, T.D. Tilley, J. Am. Chem. Soc. 124 (2002) 13194.

[20] R.L. Brutchey, C.G. Lugmair, L.O. Schebaum, T.D. Tilley, J. Catal. 229 (2005) 72.
[21] R. Rulkens, J.L. Male, K.W. Terry, B. Olthof, A. Khodakov, A.T. Bell, E. Iglesia, T.D. Tilley, Chem. Mater. 11 (1999) 2966.
[22] D.Y. Zhao, Q.S. Huo, J.L. Feng, B.F. Chmelka, G.D. Stucky, J. Am. Chem. Soc. 120 (1998) 6024.
[23] Y. Abe, I. Kijima, Bull. Chem. Soc. Jpn. 42 (1969) 1118.
[24] C. Pak, A.T. Bell, T.D. Tilley, J. Catal. 206 (2002) 49.
[25] K.L. Fujdala, T.D. Tilley, J. Am. Chem. Soc. 123 (2001) 10133.
[26] P. Van Der Voort, M. Morey, G.D. Stucky, M. Mathieu, E.F. Vansant, J. Phys. Chem. B 102 (1998) 585.
[27] S. Brunauer, P.H. Emmett, E. Teller, J. Am. Chem. Soc. 60 (1938) 309.
[28] E.P. Barrett, L.G. Joyner, P.P. Halenda, J. Am. Chem. Soc. 73 (1951) 373.
[29] N. Ohler, A.T. Bell, J. Catal. 231 (2005) 115.
[30] K.L. Fujdala, I.J. Drake, A.T. Bell, T.D. Tilley, J. Am. Chem. Soc. 126 (2004) 10864.
[31] N. Magg, B. Immaraporn, J.B. Giorgi, T. Schroeder, M. Baumer, J. Dobler, Z.L. Wu, E. Kondratenko, M. Cherian, M. Baerns, P.C. Stair, J. Sauer, H.J. Freund, J. Catal. 226 (2004) 88.
[32] S.B. Xie, E. Iglesia, A.T. Bell, Langmuir 16 (2000) 7162.
[33] C. Hess, J.D. Hoefelmeyer, T.D. Tilley, J. Phys. Chem. B 108 (2004) 9703.
[34] K. Tran, M.A. Hanninglee, A. Biswas, A.E. Stiegman, G.W. Scott, J. Am. Chem. Soc. 117 (1995) 2618.
[35] M. Morey, A. Davidson, H. Eckert, G. Stucky, Chem. Mater. 8 (1996) 486.
[36] Z.H. Luan, J.Y. Bae, L. Kevan, Chem. Mater. 12 (2000) 3202.
[37] M.D. Curran, T.E. Gedris, A.E. Stiegman, G.A. Plett, Chem. Mater. 11 (1999) 1120.
[38] U. Scharf, M. Schraml–Marth, A. Wokaun, A. Baiker, J. Chem. Soc., Faraday Trans. 87 (1991) 3299.
[39] X.T. Gao, S.R. Bare, B.M. Weckhuysen, I.E. Wachs, J. Phys. Chem. B 102 (1998) 10842.
[40] G.T. Went, S.T. Oyama, A.T. Bell, J. Phys. Chem. 94 (1990) 4240.
[41] M. Schraml-Marth, A. Wokaun, M. Pohl, H.L. Krauss, J. Chem. Soc., Faraday Trans. 87 (1991) 2635.
[42] G. Guiu, P. Grange, Bull. Chem. Soc. Jpn. 67 (1994) 2716.
[43] M.I. Osendi, J.S. Moya, C.J. Serna, J. Soria, J. Am. Ceram. Soc. 68 (1985) 135.
[44] S.M. Maurer, E.I. Ko, Catal. Lett. 12 (1992) 231.
[45] M. Baltes, K. Cassiers, P. Van Der Voort, B.M. Weckhuysen, R.A. Schoonheydt, E.F. Vansant, J. Catal. 197 (2001) 160.
[46] N. Krishnamachari, C. Calvo, Can. J. Chem. 49 (1971) 1629.
[47] M. Nabavi, F. Taulelle, C. Sanchez, M. Verdaguer, J. Phys. Chem. Solids 51 (1990) 1375.
[48] D.S.H. Sam, V. Soenen, J.C. Volta, J. Catal. 123 (1990) 417.
[49] G. Busca, G. Ricchiardi, D.S.H. Sam, J.C. Volta, J. Chem. Soc., Faraday Trans. 90 (1994) 1161.
[50] H.T. Evans, Acta Crystallogr. 13 (1960) 1019.
[51] F. Marumo, M. Isobe, S. Iwai, Y. Kondo, Acta Crystallogr. B 30 (1974) 1628.
[52] G. Centi, S. Perathoner, F. Trifiro, A. Aboukais, C.F. Aissi, M. Guelton, J. Phys. Chem. 96 (1992) 2617.
[53] X.T. Gao, I.E. Wachs, J. Phys. Chem. B 104 (2000) 1261.
[54] F. Amano, T. Tanaka, T. Funabiki, Langmuir 20 (2004) 4236.
[55] R. Pitchai, K. Klier, Catal. Rev. 28 (1986) 13.
[56] N.D. Spencer, C.J. Pereira, J. Catal. 116 (1989) 399.
[57] M.A. Bañares, M.V. Martinez-Huerta, X. Gao, J.L.G. Fierro, I.E. Wachs, Catal. Today 61 (2000) 295.
[58] M. Faraldos, M.A. Bañares, J.A. Anderson, H. Hu, I.E. Wachs, J.L.G. Fierro, J. Catal. 160 (1996) 214.
[59] R.G. Herman, Q. Sun, C.L. Shi, K. Klier, C.B. Wang, H.C. Hu, I.E. Wachs, M.M. Bhasin, Catal. Today 37 (1997) 1.